Supporting Information

Beyond ACE2: Unveiling the Receptor-Mediated Endocytic Dynamic Mechanism of SARS-CoV-2 at Single-Particle Level

Xiaoyu Ma, Zhuang Zhang, Dandan Yang, Hui Wang, Hao Zhang, Yue Yang, Siying Li and Yuping Shan**

*College of Chemistry and Life Sciences, Advanced Institute of Materials Science, Changchun University of Technology, Changchun 130012, China

†Email: lisiying@ccut.edu.cn, shanyp@ciac.ac.cn

Cell Culture

HEK 293T (human kidney epithelial cells), and HepG2 (liver cancer cells) were purchased from the Shanghai Academy of Biological Sciences. The cells were lived in Dulbecco's Modified Eagle's Medium (DMEM). The DMEM Medium was supplemented with 10% fetal bovine serum (FBS), BIOMYC-3 antibiotic (100 μg mL^{-1}), streptomycin and penicillin (100 μg mL^{-1}). Cultivation of these cells was carried out at 37 °C with 5% CO_2.

Synthesis of SARS-CoV-2 VLP-Cy3.

The complex was first dissolved in a small volume of DMSO prior to dilution in PBS. The mixture of SARS-CoV-2 VLPs and Cy3 was incubated overnight at room temperature with gentle stirring, followed by purification via ultrafiltration to yield SARS-CoV-2 VLP-Cy3 conjugates. BSG antibody-Cy5 and DPP4 antibody-Cy5 were prepared using an identical procedure.

The calculation processes of SMFS measurements.

The relationship between binding force and loading rate is characterized by an approximate equation on the basis of the single-barrier model:

$$F_u = \frac{K_B T}{X_\beta} ln\left(\frac{r X_\beta}{K_B T K_{off}}\right) = \frac{K_B T}{X_\beta} \ln r + \frac{K_B T}{X_\beta} ln\left(\frac{X_\beta}{K_B T K_{off}}\right), r = K_{eff} v \quad (1)$$

Where F_u means the unbinding force, K_B means the Boltzmann constant (1.38×10^{-2} pN·nm/K), X_β means these parathion distance from the equilibrium position, T means the Kelvin temperature (298 K), r means the loading rate, K_{off} means the dissociation kinetic rate constant at zero force, K_{eff} means the effective spring constant of the AFM tip cantilever (27.64 pN/nm), and v means the AFM tip cantilever retracting speed, all the retracting speeds are shown in the Table S4-S11. The dissociation activation energy $\Delta G_{\beta,0}$ is calculated using the following equation:

$$\Delta G_{\beta,0} = - K_B T ln\left(\tau_D K_{off}(0)\right) \quad (2)$$

Where τ_D means the diffusive relaxation time; a value of $\tau_D = 10^{-9}$ s is adopted for this expression. To calculated K_{on}, the BP is measured at different contact times. And the K_{on} is calculated using the following equation:

$$K_{on} = \frac{\frac{1}{2} \cdot 4\pi r_{eff}^3 \cdot N_A}{3 n_b \tau} \quad (3)$$

Where r_{eff} is the effective radius of the sphere, being the sum of a sphere (7.4, 8.5, and 8.1 nm for RBD, BSG antibody, and DPP4 antibody, respectively) with the equilibrium tether (r_{eff} = 3 nm for the used PEG linker) and the diameter of the RBD (4.4 nm) or corresponding antibody (BSG: 5.5 nm, DPP4: 5.1 nm), n_b means the number of binding pairs (n_b=1), and N_A means the Avogadro constant (6.022 × 10^{23} mol^{-1}), τ means the interacting duration. The BP is determined as follows:

$$BP = A * \left[1 - exp\left(\frac{-(t - t_0)}{\tau}\right)\right] \quad (4)$$

A represents the maximum BP and t_0 is the lag time, and t is a certain holding time when the AFM tip is contacting with the cell membrane. The BP is measured at 0.16, 0.32, 0.64, 0.96, 1.44, and 2.24 s, data were imported into Origin software for fitting to yield τ.

The calculation processes of the force tracing measurements.

The displacement of SARS-CoV-2 VLP cellular entry is calculated using a previously reported method. Essentially, this displacement (H) is equivalent to the sum of the AFM tip cantilever deflection (d) and the PEG linker stretching length (h):

$$H = d + h \quad (5)$$

The extended worm-like chain (WLC) model is employed to calculate the stretching length h of the PEG linker, as detailed below:

$$\frac{FL_P}{K_B T} = \frac{1}{4}\left(1 - \frac{h}{L_0} + \frac{F}{K_0}\right)^{-2} - \frac{1}{4} + \frac{h}{L_0} - \frac{F}{K_0} \quad (6)$$

In the aforementioned equation, L_p means the persistence length (4 ± 0.02 Å), K_B means the Boltzmann constant (1.380649 × 10^{-23} J/K), T means absolute temperature (298 K), L_0 means contour length, h means the extension length of the PEG linker, and K_0 means enthalpy correction (1561 ± 33 pN). Each unit of PEG is 4.2 Å, and the terminus is 5.25 Å, resulting in a contour length L_0 for PEG is nearly 333 Å. The bending distance of the AFM tip cantilever can be calculated according to Hooke's law as follows:

$$F = k \times d \quad (7)$$

Here, F corresponds to the endocytosis force derived from the FT curves, while k means the effective spring constant of the AFM tip cantilever (27.64 pN/nm). The duration t of SARS-CoV-2 VLP cell entry is retrievable from the FT curve, with the velocity v calculable by the following equation:

$$v = \frac{H}{t} \tag{8}$$

Blocking experiments.

To demonstrate that the observed FT events arise from active endocytosis, we performed additional pharmacological inhibition experiments. CPZ, 100 nM, 20 min) were utilized to pre-incubating with HEK 293T-BSG and HEK 293T-DPP4 cells, respectively. Then the cells were rigorously washed with PBS and fresh medium was replenished to conduct subsequent force tracing.

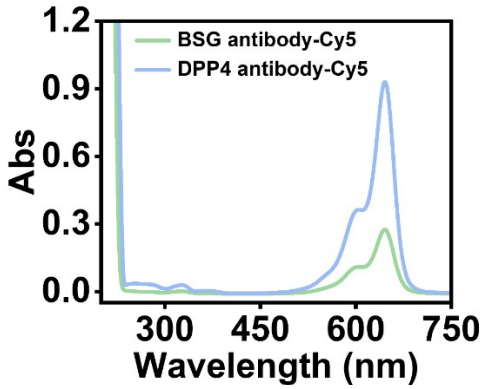

Figure S1. The characterization of BSG antibody-Cy5 and DPP4 antibody-Cy5. UV-Vis Spectra of BSG antibody-Cy5 (green), and DPP4 antibody-Cy5 (blue).

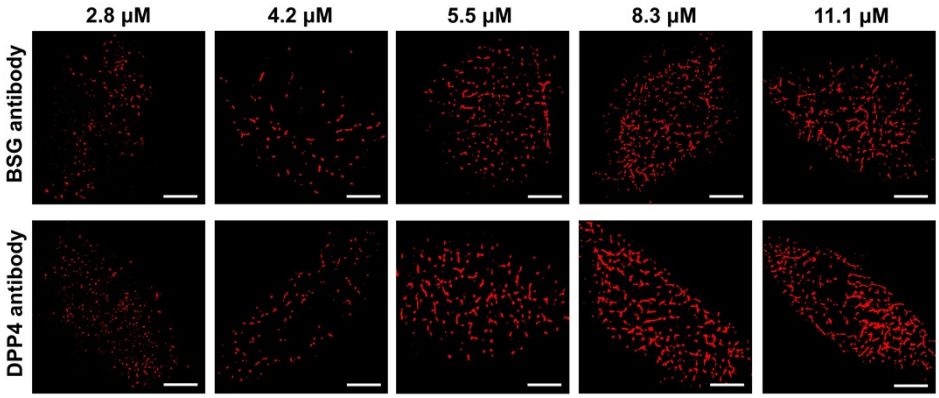

Figure S2. Representative dSTORM images of receptor labeled with the corresponding antibody at different concentrations (2.8 μM, 4.2 μM, 5.6 μM, 8.3 μM, and 11.1 μM), scale bar: 4 μm.

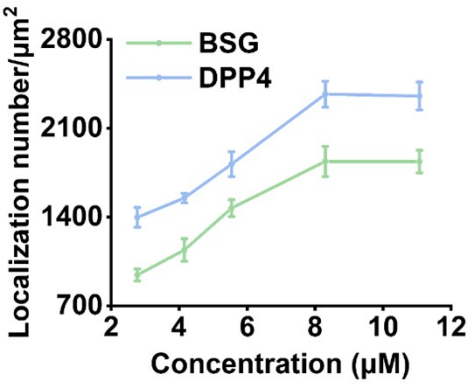

Figure S3. Localization number/μm^2 of receptor after labeled with the corresponding antibody at different concentrations (2.8 μM, 4.2 μM, 5.6 μM, 8.3 μM, and 11.1 μM).

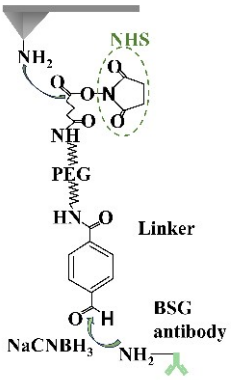

Figure S4. The antibody is attached to the AFM tip via a heterobifunctional PEG linker.

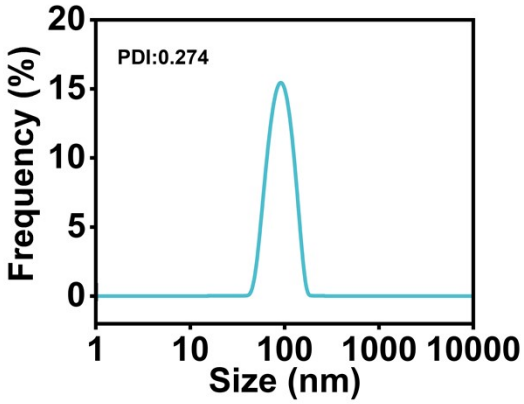

Figure S5. Particle size distribution of SARS-CoV-2 VLP determined by the dynamic light scattering (DLS) technique.

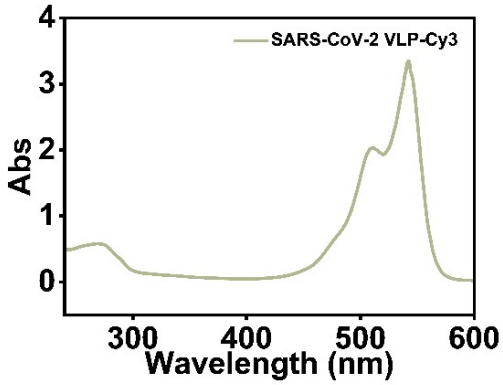

Figure S6. The characterization of SARS-CoV-2 VLP-Cy3. UV-Vis Spectra of SARS-CoV-2 VLP-Cy3.

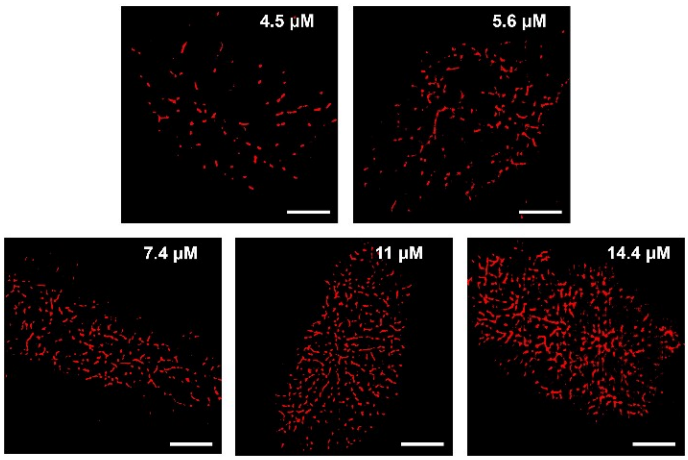

Figure S7. Representative dSTORM images of BSG labeled with SARS-CoV-2 VLPs at different concentrations (4.5 μM, 5.6 μM, 7.4 μM, 11.0 μM, and 14.4 μM) after the HepG2 cell were incubated with DPP4 antibody, scale bar: 4 μm.

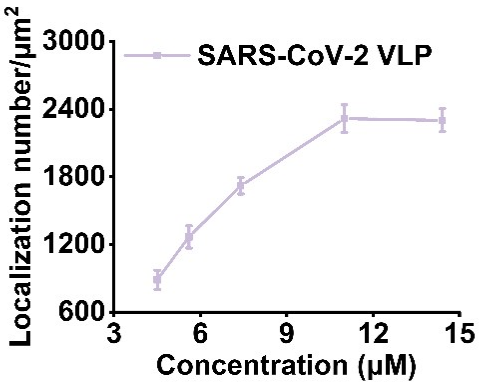

Figure S8. Localization number/μm^2 of BSG after labeled with SARS-CoV-2 VLPs at different concentrations (4.5 μM, 5.6 μM, 7.4 μM, 11.0 μM, and 14.4 μM).

Table S1. Kinetic parameters characterizing the interaction between corresponding antibody and receptor.

	τ (s)	K_{on} (M^{-1} s^{-1})	K_{off} (s^{-1})	K_a (M^{-1})	K_d (M)	X_β (nm)	$\Delta G_{\beta,0}$ (K_BT)
BSG antibody-BSG	0.20	4.44×10^{4}	0.19×10^{-3}	2.34×10^{8}	0.43×10^{-8}	0.18	29.29
DPP4 antibody-DPP4	0.20	1.20×10^{5}	0.12×10^{-3}	9.68×10^{8}	0.10×10^{-8}	0.18	29.72

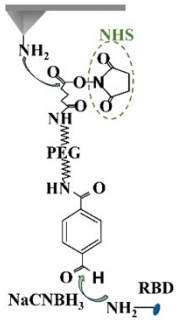

Figure S9. The RBD is attached to the AFM tip via a heterobifunctional PEG linker.

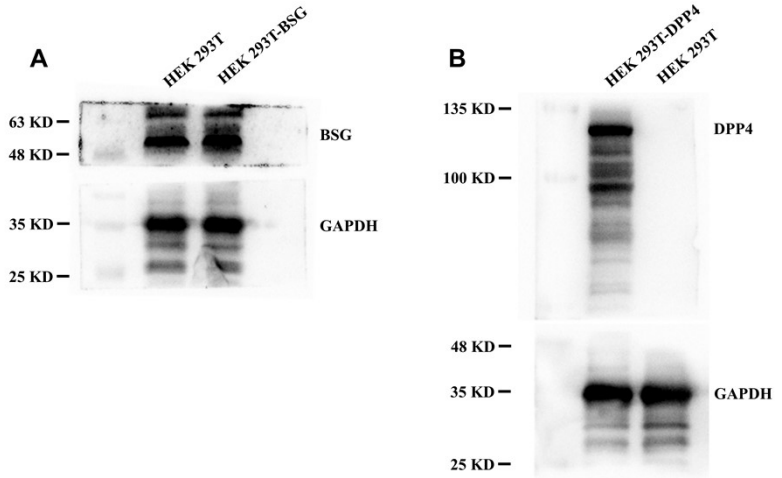

Figure S10. Western blot of BSG (A) and DPP4 (B) expression levels in transfected cell.

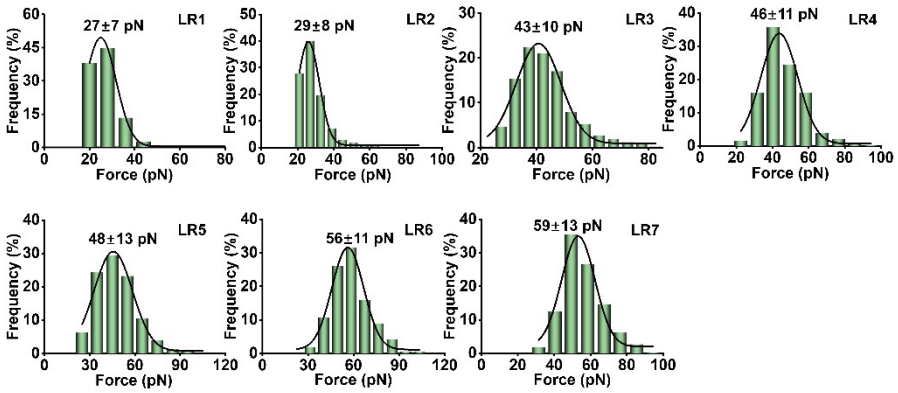

Figure S11. The histogram distributions of unbinding forces for RBD-BSG. The LRs (from Figure 3D) are divided into narrow LR ranges 1-7. The distribution of unbinding forces located in small LR is plotted as histograms and fitted by multipeak Gaussian fits.

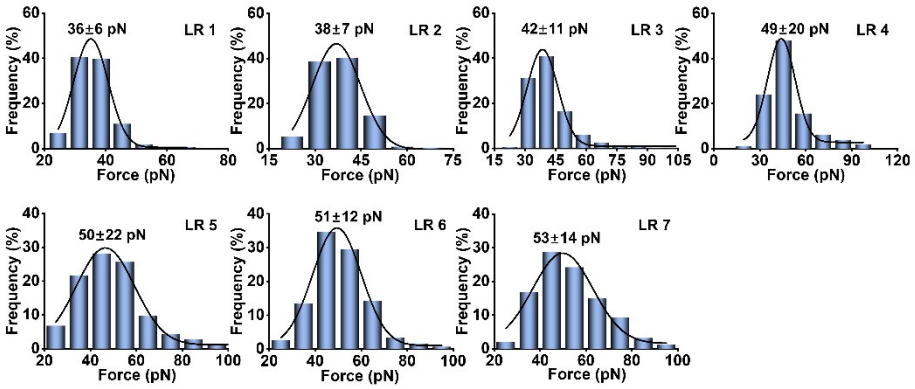

Figure S12. The histogram distributions of unbinding forces for RBD-DPP4. The LRs (from Figure 3D) are divided into narrow LR ranges 1-7. The distribution of unbinding forces located in small LR is plotted as histograms and fitted by multipeak Gaussian fits.

Table S2. Kinetic parameters characterizing the interaction between RBD or corresponding antibody and receptor.

	τ (s)	K_{on} (M^{-1} s^{-1})	K_{off} (s^{-1})	K_a (M^{-1})	K_d (M)	X_β (nm)	$\Delta G_{\beta,0}$ (K_BT)
RBD-BSG	0.23	3.91×10^{4}	0.21×10^{-3}	1.86×10^{8}	0.54×10^{-8}	0.22	29.19
RBD-DPP4	0.23	3.89×10^{4}	0.48×10^{-3}	0.81×10^{8}	1.23×10^{-8}	0.31	28.37
BSG antibody-BSG	0.22	4.00×10^{4}	0.20×10^{-3}	2.02×10^{8}	0.50×10^{-8}	0.19	29.22
DPP4 antibody-DPP4	0.21	1.14×10^{5}	0.15×10^{-3}	7.60×10^{8}	0.13×10^{-8}	0.17	29.53

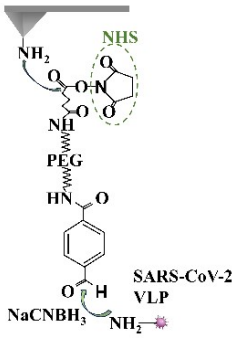

Figure S13. The SARS-CoV-2 VLP is attached to the AFM tip via a heterobifunctional PEG linker.

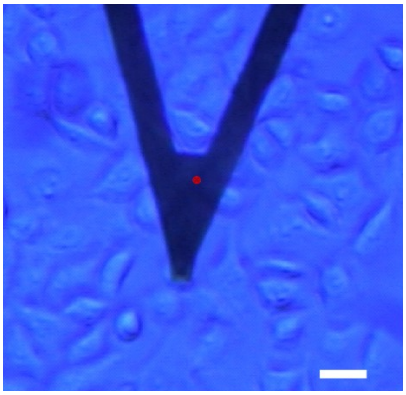

Figure S14. The optical image of the AFM tip cantilever locating above the living HEK 293T cells, Scale bar: 50 μm.

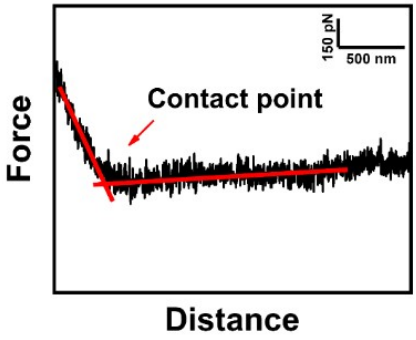

Figure S15. The contact point between the SARS-CoV-2 VLP modified AFM tip and the cell surface. The contact point is the intersection of the slope (red line) and the flat part in the FD curve.

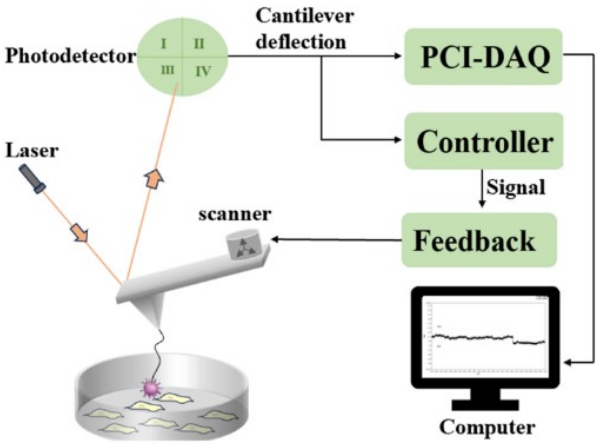

Figure S16. Schematic diagram of the force tracing technique workflow.

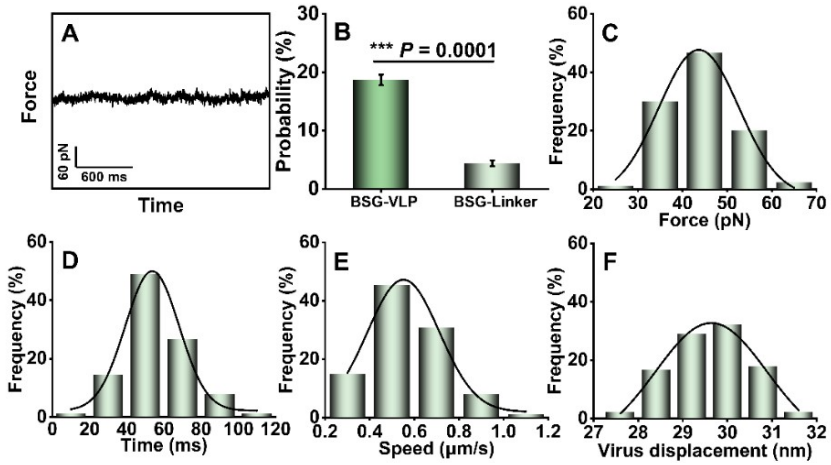

Figure S17. Force tracing measurements of PEG linker internalization in HEK 293T-BSG. (A) The typical FT curve. (B) Probability of observing FT signals for PEG linker (n = 90), and SARS-CoV-2 VLP (n = 397) through BSG. The probability was calculated from more than three independent experiments, respectively. (C-F) Required force, duration, speed, and displacement distribution histogram for PEG linker entry cell, respectively. The *P* value was compared using unpaired two-tailed Student's *t* test. ***$P \leq 0.001$.

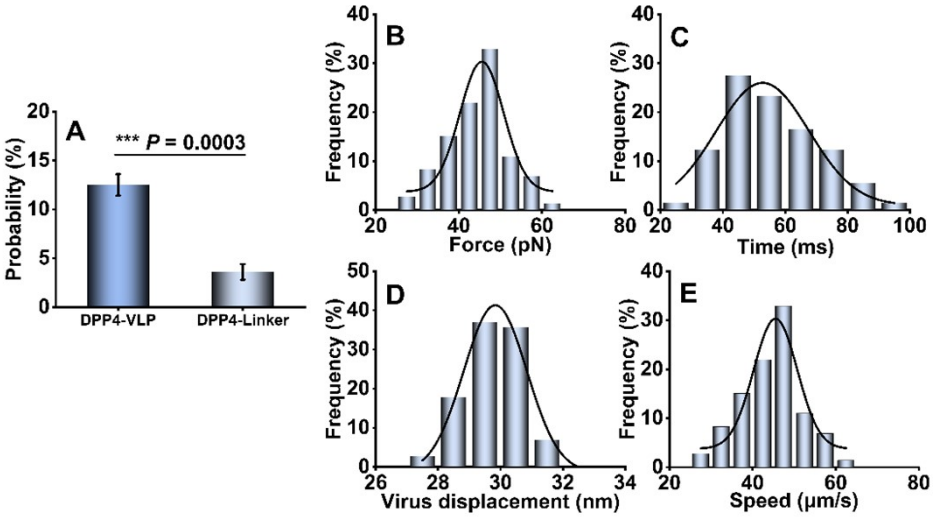

Figure S18. Force tracing measurements of PEG linker internalization in HEK 293T-DPP4. (A) Probability of observing FT signals for PEG linker (n = 73), and SARS-CoV-2 VLP (n = 325) through DPP4. The probability was calculated from more than three independent experiments, respectively. (B-E) Required force, duration, speed, and displacement distribution histogram for PEG linker entry cell, respectively. The *P* value was compared using unpaired two-tailed Student's *t* test. ***$P \leq 0.001$.

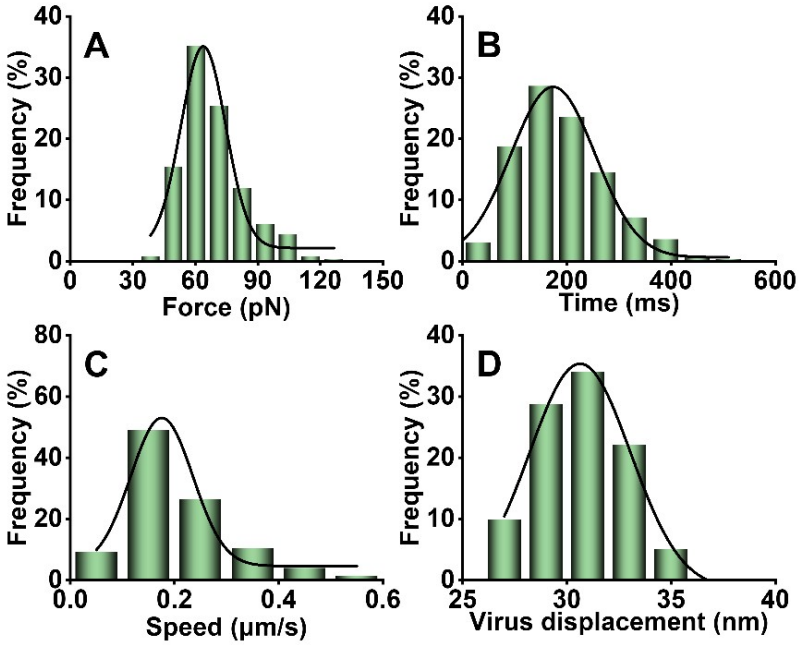

Figure S19. The force, duration, speed, and displacement for single SARS-CoV-2 VLP entry HEK 293T-BSG cell. (A-D) Required force, duration, speed, and displacement distribution histogram for SARS-CoV-2 VLP entry cell, respectively.

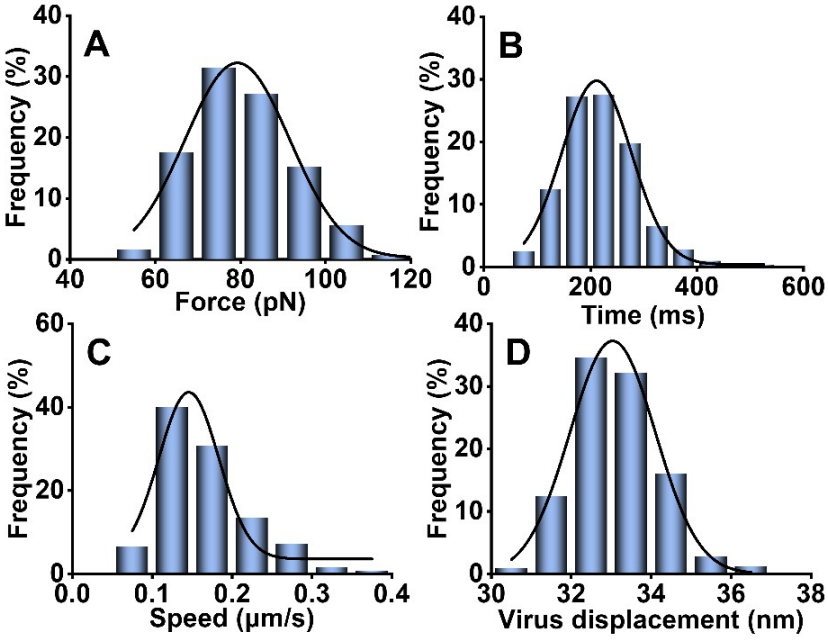

Figure S20. The force, duration, speed, and displacement for single SARS-CoV-2 VLP entry HEK 293T-DPP4 cell. (A-D) Required force, duration, speed, and displacement distribution histogram for SARS-CoV-2 VLP entry cell, respectively.

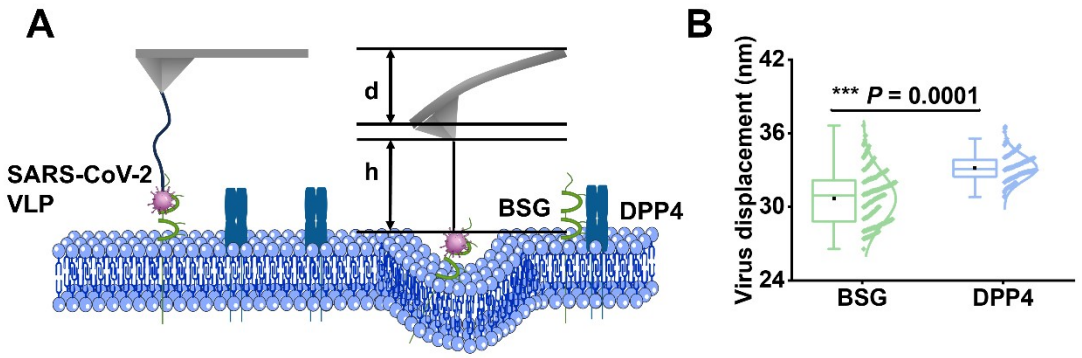

Figure S21. Calculating the displacement during the process of SARS-CoV-2 VLP entry cell. (A) Schematic of the displacement during the process of SARS-CoV-2 VLP entry cell, consisting the bending distance of the AFM tip cantilever (d) and the extension length of the PEG linker (h). (B) The box plot statistical analysis of entry cell displacement for BSG and DPP4 mediated SARS-CoV-2 VLP entry, respectively. The boxes mean the main distribution (50%) of values, the vertical lines through boxes represent the 5% to 95% data range, the horizontal lines in every box represent the median, and the square in every box is the mean value. The *P* value was compared using unpaired two-tailed Student's *t* test. ***$P \leq 0.001$.

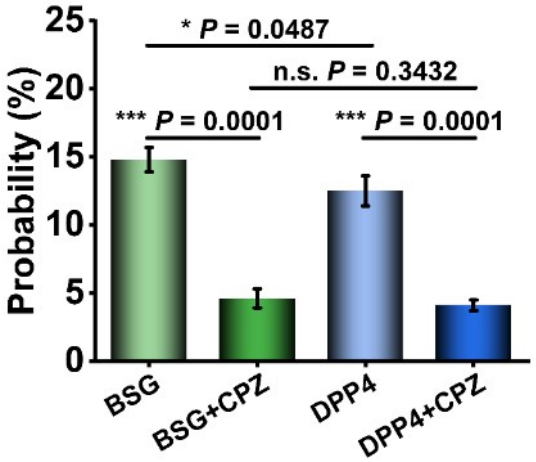

Figure S22. Probability of capturing FT signal before and after inhibition, which is the mean value from more than three individual groups. For each group, 2000 randomly selected curves are analyzed, dividing the sum of force curves appearing signal by 2000, the value is expressed as mean ± s.d. The *P* value was compared using unpaired two-tailed Student's *t* test. n.s.: no significant, *$P \leq 0.1$, ***$P \leq 0.001$.

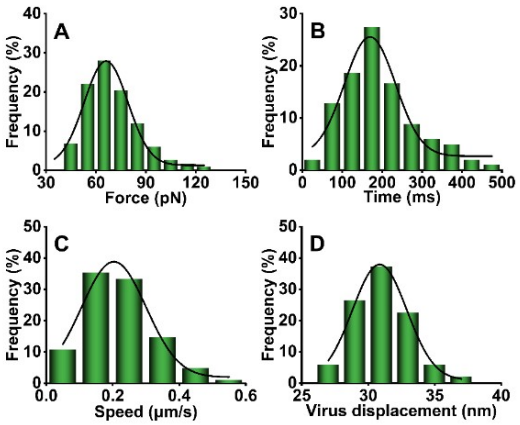

Figure S23. The force (A), duration (B), speed (C), and displacement (D) distribution histogram after blocking with CPZ in HEK 293T-BSG cell.

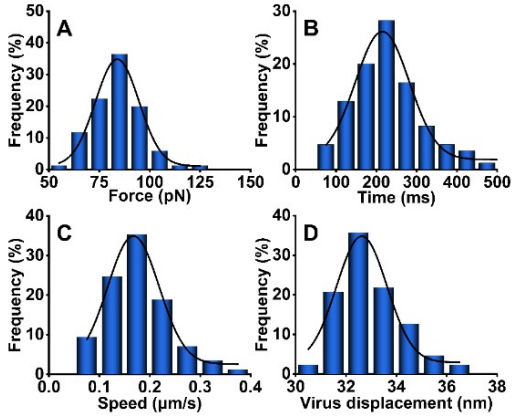

Figure S24. The force (A), duration (B), speed (C), and displacement (D) distribution histogram after blocking with CPZ in HEK 293T-DPP4 cell.

Table S3. Kinetic parameters characterizing the interaction between RBD (with or without TCEP pretreatment) and receptor.

	τ (s)	K_{on} (M^{-1} s^{-1})	K_{off} (s^{-1})	K_a (M^{-1})	K_d (M)	X_β (nm)	$\Delta G_{\beta,0}$ (K_BT)
RBD+TCEP-BSG	0.28	3.22×10^{4}	0.27×10^{-3}	1.19×10^{8}	0.81×10^{-8}	0.36	28.94
RBD-BSG	0.23	3.91×10^{4}	0.21×10^{-3}	1.86×10^{8}	0.54×10^{-8}	0.22	29.19
RBD+TCEP-DPP4	0.28	3.18×10^{4}	7.41×10^{-3}	0.43×10^{7}	2.30×10^{-7}	0.47	25.63
RBD-DPP4	0.23	3.89×10^{4}	0.48×10^{-3}	0.81×10^{8}	1.23×10^{-8}	0.31	28.37

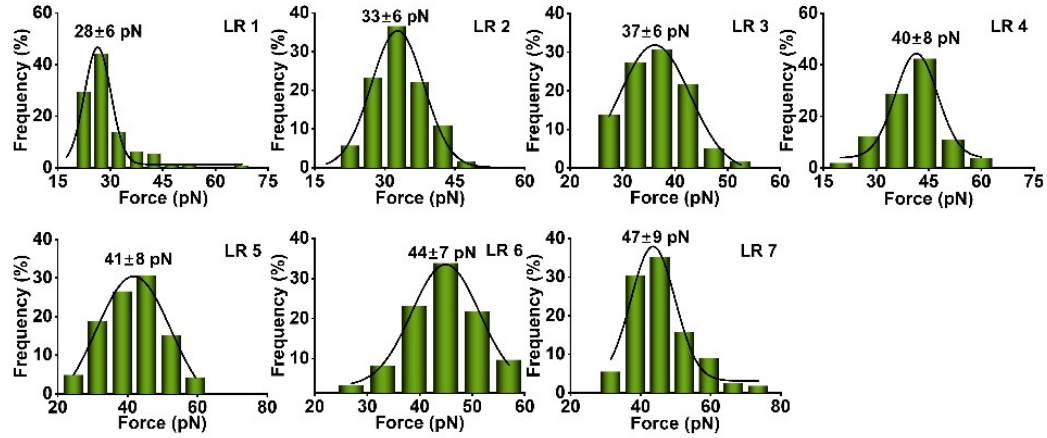

Figure S25. The histogram distributions of unbinding forces for RBD+TCEP-BSG. The LRs (from Figure 6D) are divided into narrow LR ranges 1-7. The distribution of unbinding forces located in small LR is plotted as histograms and fitted by multipeak Gaussian fits.

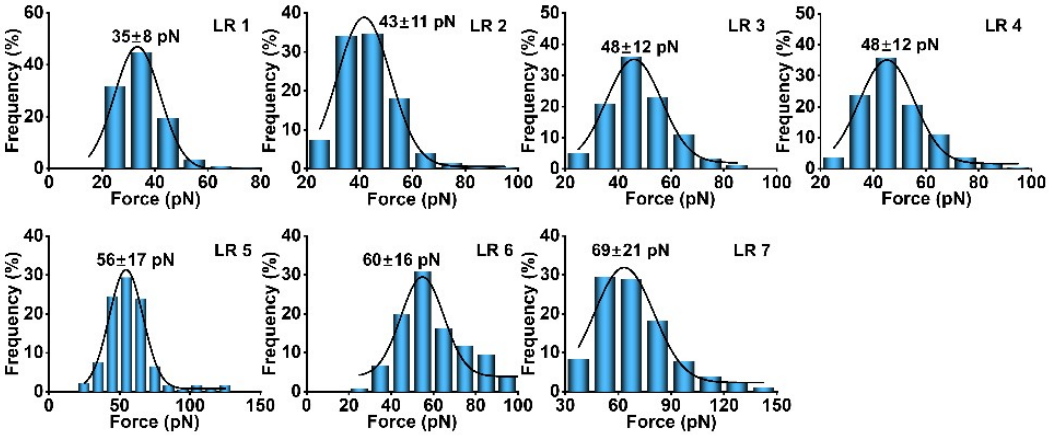

Figure S26. The histogram distributions of unbinding forces for RBD+TCEP-DPP4. The LRs (from Figure 6D) are divided into narrow LR ranges 1-7. The distribution of unbinding forces located in small LR is plotted as histograms and fitted by multipeak Gaussian fits.

Table S4. Experimental AFM tip cantilever retracting rate, loading rate, and LnR parameters for BSG antibody-BSG interaction in HepG2 cell.

Retracting rate (μm/s)	Loading rate (pN s^{-1})	LnR (pN s^{-1})
4.2	2.0×10^3	7.6
6.6	3.3×10^3	8.1
8.4	4.0×10^3	8.3
10.8	5.4×10^3	8.6
14.5	7.2×10^3	8.9
16.1	8.1×10^3	9.0
17.8	8.9×10^3	9.1

Table S5. Experimental AFM tip cantilever retracting rate, loading rate, and LnR parameters for DPP4 antibody-DPP4 interaction in HepG2 cell.

Retracting rate (μm/s)	Loading rate (pN s^{-1})	LnR (pN s^{-1})
4.2	4.5×10^3	8.4
6.5	7.2×10^3	8.9
8.3	9.0×10^3	9.1
16.5	1.8×10^4	9.8
18.2	2.0×10^4	9.9
20.0	2.2×10^4	10.0
21.8	2.4×10^4	10.1

Table S6. Experimental AFM tip cantilever retracting rate, loading rate, and LnR parameters for RBD-BSG interaction in HEK 293T-BSG cell.

Retracting rate (μm/s)	Loading rate (pN s^{-1})	LnR (pN s^{-1})
2.5	1.7×10^3	7.4
3.1	2.2×10^3	7.7
4.2	2.9×10^3	8.0
6.3	4.3×10^3	8.4
8.3	5.7×10^3	8.7
10.4	7.2×10^3	8.9
12.5	8.6×10^3	9.1

Table S7. Experimental AFM tip cantilever retracting rate, loading rate, and LnR parameters for RBD-DPP4 interaction in HEK 293T-DPP4 cell.

Retracting rate (μm/s)	Loading rate (pN s^{-1})	LnR (pN s^{-1})
4.2	2.1×10^3	7.7
6.3	3.2×10^3	8.1
8.3	4.2×10^3	8.4
10.5	5.3×10^3	8.6
12.9	6.6×10^3	8.8
14.5	7.2×10^3	8.9
16.1	8.3×10^3	9.0

Table S8. Experimental AFM tip cantilever retracting rate, loading rate, and LnR parameters for DPP4 antibody-DPP4 interaction in HEK 293T-BSG cell.

Retracting rate (μm/s)	Loading rate (pN s^{-1})	LnR (pN s^{-1})
4.2	1.5×10^3	7.3
6.3	2.2×10^3	7.7
7.0	2.4×10^3	7.8
8.6	3.0×10^3	8.0
9.5	3.3×10^3	8.1
10.5	3.7×10^3	8.2
20.5	7.2×10^3	8.9

Table S9. Experimental AFM tip cantilever retracting rate, loading rate, and LnR parameters for DPP4 antibody-DPP4 interaction in HEK 293T-DPP4 cell.

Retracting rate (μm/s)	Loading rate (pN s^{-1})	LnR (pN s^{-1})
4.2	2.7×10^3	7.9
6.3	4.0×10^3	8.3
11.4	7.2×10^3	8.9
12.9	8.1×10^3	9.0
14.3	9.0×10^3	9.1
19.0	1.2×10^4	9.4
20.5	1.3×10^4	9.5

Table S10. Experimental AFM tip cantilever retracting rate, loading rate, and LnR parameters for RBD+TCEP-BSG interaction in HEK 293T-BSG cell.

Retracting rate (μm/s)	Loading rate (pN s^{-1})	LnR (pN s^{-1})
4.2	2.7×10^3	7.9
6.2	4.0×10^3	8.3
8.3	5.4×10^3	8.6
10.5	7.2×10^3	8.9
12.5	8.1×10^3	9.0
14.5	9.0×10^3	9.1
22.5	1.5×10^4	9.6

Table S11. Experimental AFM tip cantilever retracting rate, loading rate, and LnR parameters for RBD+TCEP-DPP4 interaction in HEK 293T-DPP4 cell.

Retracting rate (μm/s)	Loading rate (pN s^{-1})	LnR (pN s^{-1})
4.2	1.0×10^3	6.9
6.2	2.0×10^3	7.6
8.3	3.0×10^3	8.0
10.5	5.4×10^3	8.6
12.5	6.0×10^3	8.7
20.5	2.4×10^4	10.1
22.5	2.4×10^4	10.1